JOURNAL OF GUIDANCE, CONTROL, AND DYNAMICS
Vol. 23, No. 1, January–February 2000

Precision Spacecraft Pointing Using Single-Gimbal Control Moment Gyroscopes with Disturbance

Christopher J. Heiberg* and David Bailey†
Honeywell, Inc., Phoenix, Arizona 85382
and
Bong Wie‡
Arizona State University, Tempe, Arizona 85287-6016

Whereas previous work has shown that gain stabilization methods in the attitude control of spacecraft can mitigate external disturbances of a fixed frequency, recent work in cases where the frequency of the disturbance is time variant is summarized here. Specifically, the application of gain stabilization in the form of a variable periodic disturbance rejection filter is shown to be a viable method of mitigating these disturbances. To use this filter for the time-variant case, the character of the source of the disturbance needs to be known a priori with some accuracy. An implementation for a spacecraft steered by single-gimbal control moment gyroscopes where the disturbance is related to the gimbal rate is demonstrated. In addition, performance of the subject filter is demonstrated in the presence of estimation error and phase shift.

Introduction

SINGLE-GIMBAL control moment gyroscopes (SGCMGs) store angular momentum that can be extracted on demand through the precession of the angular momentum vector. SGCMGs manifest the momentum vector in a rotating inertial mass contained in a gimbal that is supported by high-capacity bearings. A gimbal torquer module is used to produce the commanded gimbal rotation. The primary advantage SGCMGs have over other torque-producing devices is torque amplification; output torque resulting from rotation of the stored momentum vector is much greater than what is required to produce gimbal motion. However, angular speed variations in the gimbal torquer, and thereby the gimbal itself, are also amplified and transmitted to the satellite as a disturbance commonly called torque ripple. Frequency content of the torque ripple is generally predictable; however, due to its dependence on the gimbal angular rate, it tends to vary over a broad frequency range. Inevitably, disturbance frequencies or their harmonics will coincide with critical structural modes of the spacecraft bus or payload. To further complicate matters, any SGCMG disturbance frequency content identified during ground testing can differ significantly when devices are mounted in a flexible spacecraft structure and placed in orbit.

The nature of SGCMG disturbances will be shown to be basically periodic, but of a time-varying nature. It has been shown that fixed external periodic disturbances acting on a spacecraft cannot be eliminated using conventional controller design without the presence of an internal model of the disturbance in the controller.[1] In the case of the Hubble space telescope (HST), disturbances due to solar panel modes rendered the instrument incapable of being utilized to its full potential. Rejection of periodic disturbances in the HST was demonstrated by adding a model of disturbance in the controller, thereby providing additional loop gain at the disturbance frequency; subsequently, the pointing error was asymptotically driven to zero.[2] The disturbance on the HST was essentially external to the platform, and its nature and frequency were well understood. In Ref. 3, the same principle was applied for external periodic disturbances where the frequencies were not fixed and the disturbances were both external and internal to the platform.

Received 19 March 1998; revision received 26 May 1999; accepted for publication 28 May 1999.

*Staff Engineer, Guidance Navigation and Control, Satellite Systems Operation, P.O. Box 52199.
†Senior Staff Engineer, Guidance Navigation and Control.
‡Professor, Department of Mechanical and Aerospace Engineering.

This paper will take a closer look at the sources of these disturbances and suggest some representative models. In addition, mitigation of these disturbances will be attempted. This will be evaluated in two stages, and the methods previously presented in Ref. 3 will be further evaluated on external disturbances and then applied to the internal ones. First, the model that is used along with the controller characteristics is described. The remaining sections describe the disturbances, mitigation, and results of the models.

Spacecraft and Control Moment Gyroscope (CMG) Dynamics

The equation of motion of a rigid spacecraft with momentum exchange actuators is given by the following equation:

$$\dot{\boldsymbol{H}}_S + \boldsymbol{\omega} \times \boldsymbol{H}_S = \boldsymbol{T}_{\text{ext}} \tag{1}$$

where $\boldsymbol{H}_S = (H_{S1}, H_{S2}, H_{S3})$ is the total angular momentum vector of the spacecraft expressed in the spacecraft body-fixed control axes, and $\boldsymbol{T}_{\text{ext}}$ is the external torque vector including the gravity gradient, solar pressure, and aerodynamic torques (expressed in the same axes). The total angular momentum vector consists of the spacecraft main body angular momentum and the CMG angular momentum; that is, we have

$$\boldsymbol{H}_S = \boldsymbol{J}\boldsymbol{\omega} + \boldsymbol{h} \tag{2}$$

where $\boldsymbol{J}$ is the inertia matrix of the spacecraft including CMGs, $\boldsymbol{\omega} = (\omega_1, \omega_2, \omega_3)$ is the spacecraft angular velocity vector, and $\boldsymbol{h} = (h_1, h_2, h_3)$ is the CMG momentum vector expressed in the spacecraft body-fixed control axes. Combining Eqs. (1) and (2), we obtain

$$(\boldsymbol{J}\dot{\boldsymbol{\omega}} + \dot{\boldsymbol{h}}) + \boldsymbol{\omega} \times (\boldsymbol{J}\boldsymbol{\omega} + \boldsymbol{h}) = \boldsymbol{T}_{\text{ext}} \tag{3}$$

Furthermore, by introducing the internal control torque vector generated by CMGs, Eq. (3) simplifies to

$$\boldsymbol{J}\dot{\boldsymbol{\omega}} + \boldsymbol{\omega} \times \boldsymbol{J}\boldsymbol{\omega} = \boldsymbol{u} + \boldsymbol{T}_{\text{ext}} \tag{4}$$

and

$$\dot{\boldsymbol{h}} + \boldsymbol{\omega} \times \boldsymbol{h} = -\boldsymbol{u} \tag{5}$$

Various attitude control and CMG momentum management systems can be designed by augmenting these equations with an additional set of kinematic differential equations concerning quaternions, Gibbs parameters, or Euler angles. Consequently, spacecraft

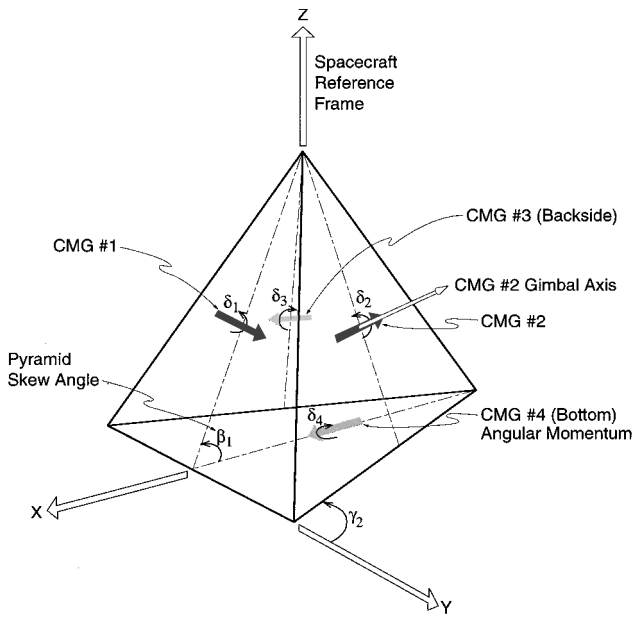

Fig. 1 Four CMG array in a three-sided pyramid orientation (three sides and one on bottom).

control torque input $\boldsymbol{u}$ can be assumed to be known for the subsequent steering logic design, and the desired CMG momentum rate is often selected as

$$\dot{\boldsymbol{h}} = -\boldsymbol{u} - \omega \times \boldsymbol{h} \tag{6}$$

The CMG angular momentum vector $\boldsymbol{h}$ is, in general, a function of CMG gimbal angles; that is, $\boldsymbol{\delta} = (\delta_1, \ldots, \delta_n)$ and $\boldsymbol{h} = \boldsymbol{h}(\delta)$. The time derivative of $\boldsymbol{h}$ is then expressed as

$$\dot{\boldsymbol{h}} = \boldsymbol{A}(\delta)\dot{\delta} \tag{7}$$

where

$$\boldsymbol{A} = \frac{\partial \boldsymbol{h}}{\partial \delta} \equiv \left[\frac{\partial h_i}{\partial \delta_j}\right] \tag{8}$$

is a $3 \times n$ Jacobian matrix. The direction of $\boldsymbol{h}$ is obtained by taking the cross product of the unit vectors normal to CMG momentum planes (CMG gimbal axis directions) with the unit vectors defining the gimbal angles with respect to their reference (Fig. 1). Note that the reference gimbal angles are selected such that initially they are mutually perpendicular to the momentum vector (rotor spin axis) and the gimbal axes. Magnitudes associated with $\boldsymbol{h}$ are found from the individual CMG rotor inertia and instantaneous operating speed.

The CMG steering logic design is simply to find an inversion of $\boldsymbol{A}\dot{\delta} = \dot{\boldsymbol{h}}$, that is, to determine gimbal rates that deliver the commanded $\dot{\boldsymbol{h}}$, while meeting hardware constraints and avoiding singularities. Note that in this CMG steering problem formulation, gimbal torquer dynamics, that is effects of gimbal axis inertia, off-axis coupling, spin vector variation, and structural dynamics, have been ignored because they are typically much smaller than the control torque output generated by CMGs. However, because CMG gimbal dynamics can be significant, an approximation of the CMG is utilized. This is simply modeled as a low-pass filter,

$$\omega^2/(s^2 + 2\xi\omega s + \omega^2) \tag{9}$$

where $\xi = 0.707$ and $\omega = 20\pi$ (10-Hz CMG loop bandwidth).

Steering Control Law for SGCMGs

Consider a pyramid mounting arrangement of four SGCMGs, as shown in Fig. 1, in which CMG momentum vectors are constrained to the faces of a three-sided pyramid with the momentum plane of the fourth CMG serving as the bottom. The angle that the momentum planes are rotated from the base is called the skew angle β_i. Gimbal axes of the four CMGs are normal to the pyramid faces, and the gimbal angles of the CMGs from the reference are denoted by δ_i. The last angle defined is the rotation of the plane about the z axis, γ_i. The system used in this paper is set up to resemble a pyramid with its apex in the yaw axis resulting in $\beta = (60, 180, 300, 0)$ deg and $\gamma = (0, 0, 0, 0)$ deg. Each CMG is assumed to have the same angular momentum h_0, about its rotor spin axis. This minimally redundant SGCMG configuration presents a significant challenge for developing singularity-robust steering laws.[4] With $\delta_0 = (35.1, -29.5, -4.8, -59.9)$ deg, the CMG array has a $1h_0$ momentum bias in the pitch axis (where h_0 is the momentum of a single CMG).

For a chosen or commanded control torque input $\boldsymbol{u}$, the CMG momentum rate command $\dot{\boldsymbol{h}}$ is determined as in Eq. (6), and the gimbal rate command $\dot{\delta}$ may be obtained as follows:

$$\dot{\delta} = \boldsymbol{A}^+\dot{\boldsymbol{h}} = \boldsymbol{A}^T(\boldsymbol{A}\boldsymbol{A}^T)^{-1}\dot{\boldsymbol{h}} \tag{10}$$

where $\boldsymbol{A}^+$ is the pseudoinverse of $\boldsymbol{A}$, often referred to as the Moore–Penrose pseudoinverse. Most CMG steering laws determine gimbal rate commands with some variant of the Moore–Penrose pseudoinverse.[3–8]

However, if rank $(\boldsymbol{A}\boldsymbol{A}^T)$ is less than three for certain sets of gimbal angles, the pseudoinverse does not exist, and the steering logic encounters singular states. This singular situation occurs when all individual CMG torque outputs are perpendicular to the singular direction. Note that for any system of n CMGs, there are 2^n sets of singular gimbal angles, for which no control torque can be generated along particular axes.[4,6,9] The result is a loss of control in an axis perpendicular to the plane. In general, there are two types of singular states: 1) hyperbolic states that can be escaped through null motion and 2) elliptic states that cannot be escaped through null motion.[9] Elliptic singular states pose a major difficulty with SGCMG systems because they are considered inescapable. Further treatment of various pseudoinverse-based steering logic for SGCMG systems are available,[4–15] and will not be discussed here. Steering logic tends to allow the system to be driven to singular states because the pseudoinverse $\boldsymbol{A}^+ = \boldsymbol{A}^T(\boldsymbol{A}\boldsymbol{A}^T)^{-1}$ is in fact the minimum two-norm vector solution. An approach to mitigating detrimental effects of singular states is to employ a singularity-robust inverse as follows:[12]

$$\dot{\delta} = \boldsymbol{A}^T(\boldsymbol{A}\boldsymbol{A}^T + k\boldsymbol{I})^{-1}\dot{\boldsymbol{h}} \tag{11}$$

where $\boldsymbol{I}$ is an identity matrix and k is a small positive scalar constant to be properly adjusted. Note that the particular solution obtained from this singularity-robust inverse approach is still orthogonal to the homogeneous solution. However, through singular value decomposition, this can be shown to result in a condition where the gimbal rate commands go to zero when a singular state is encountered. Although this is a safe condition when compared to having infinite gimbal rates if k were set to zero, the spacecraft is out of control until a different torque command is issued.

An agile spacecraft would typically be required to perform many different maneuvers; however, the one of greatest interest here is the long duration rest-to-rest slew maneuver. In this maneuver, the desired controller would achieve smooth eigenaxis rotation, during which precision pointing is being performed. The same controller must also be capable of stabilizing the platform when no rotation is desired.

Spacecraft Attitude Control Logic

To achieve a rest-to-rest eigenaxis rotation, with maximum acceleration and a constant slew rate, the controller will utilize cascade-saturation control logic.[16] This will result in the desired maneuver without exceeding prescribed spacecraft rate limits and without saturating the CMGs. The controller will also utilize quaternion feedback where the quaternions are associated with an eigenaxis rotation about an Euler axis. For the reduction of the differential equations, the quaternion vector is denoted as $\boldsymbol{q} = (q_1, q_2, q_3)$ and q_4 is a generated angle.

The quaternion kinematic differential equations are given by

$$\dot{\boldsymbol{q}} = -\tfrac{1}{2}\omega \times \boldsymbol{q} + \tfrac{1}{2}q_4\omega \tag{12}$$

$$\dot{q}_4 = -\tfrac{1}{2}\omega^T\boldsymbol{q} \tag{13}$$

It is desired to implement the cascading saturation control so that the spacecraft does not exceed a prescribed rate about any axis. In addition, control commands need to be specified such that the CMGs do not exceed a prescribed gimbal rate. These constraints are achieved through a saturation function described as follows:

$$\underset{\sigma}{\text{sat}}(\boldsymbol{x}) = \begin{cases} \boldsymbol{x} & \text{if} \quad \sigma(\boldsymbol{x}) < 1 \\ \boldsymbol{x}/\sigma(\boldsymbol{x}) & \text{if} \quad \sigma(\boldsymbol{x}) \geq 1 \end{cases} \tag{14}$$

where $\sigma(\boldsymbol{x})$ is a positive scalar function of $\boldsymbol{x}$ that characterizes the largeness of the vector $\boldsymbol{x}$. In this case, the norm of the vector will be used as the positive scalar function.

The torque command is generated as follows:

$$\boldsymbol{u}_C = -\underset{\sigma}{\text{sat}}[\boldsymbol{K}\ \text{sat}(\boldsymbol{Pq}) + \boldsymbol{C}\omega] \tag{15}$$

where $\boldsymbol{K}$, $\boldsymbol{P}$, and $\boldsymbol{C}$ are controller gains defined by

$$\boldsymbol{K} = \text{diag}(k_1, k_2, k_3)\boldsymbol{J} \tag{16}$$

$$\boldsymbol{P} = \boldsymbol{K}^{-1}k\boldsymbol{J} \tag{17}$$

$$\boldsymbol{C} = c\boldsymbol{J} \tag{18}$$

and

$$k_i = c\frac{|q_i(0)|}{\|\boldsymbol{q}(0)\|}\omega_{\max} \tag{19}$$

$$k = 2\omega_n^2 \tag{20}$$

$$c = 2\xi\omega_n \tag{21}$$

where ω_n is the desired spacecraft control bandwidth, ξ is the desired damping ratio for the rest-to-rest maneuver, and only the diagonal elements of $\boldsymbol{J}$ are used. The specific values used in this analysis are as follows:

$$\boldsymbol{J} = \begin{bmatrix} 2331 & 0 & 0 \\ 0 & 2331 & 0 \\ 0 & 0 & 777 \end{bmatrix} \text{ft} \cdot \text{lb-s}^2$$

$\omega_{\max} = 0.017r/s$ (1 deg/s), $\omega_n = 1.0$ Hz, $\xi = 2$, and $h_0 = 35$ ft · lb-s. Note that when products of inertia show up in $\boldsymbol{J}$, the gyroscopic cross coupling generates off-axis torque that is sensed as a disturbance by rate sensors and that is easily accommodated under this control.

The system model is illustrated in a MATLAB® Simulink® block diagram in Fig. 2.

SGCMG Disturbance Description

The higher spacecraft precession rates unique to agile spacecraft result in high-torque demand from the gimbal torquer module due to gyroscopic cross coupling. To efficiently accommodate this demand, torquer modules typically contain a gear transmission to multiply the motor torque. The most common torquer module designs are angular rate loop controlled devices. The sources of rate-dependent disturbances in SGCMGs are easily grouped into two categories: 1) mechanical and 2) electromechanical. Although it is recognized that electronic noise can also be a contributor, for the scope of this discussion, disturbance sources will be limited to the two most common sources listed.

Electromechanical disturbances include motor cogging, motor back electromotive forces (BEMF), commutation or switching errors, and other electrical errors that are within the torquer control feedback loop. However, the most pervasive electromechanical error comes from the gimbal rate tachometer. This error manifests itself in a manner similar to sensor noise and is not controllable by the torquer itself.

The primary mechanical source of torquer rate ripple is the speed reduction gears and their supporting rotating elements. Gimbal and torquer bearings can also provide rate variations due to varying friction and race defects; however, they tend to be more than an order of magnitude less than the gear transmission errors.

Electromagnetic Errors

Tachometers typically consist of a fixed stator and a rotating magnetic rotor. A voltage signal proportional to angular rate is produced as the rotating magnet passes the windings in the stator. Signal errors can arise from commutation switching, from physical imperfections in the windings, or in the geometry of the rotor and stator structures. Typically, space-rated devices are meticulously hand assembled and tested to minimize such errors, but the errors cannot be completely eliminated. Nonhomogeneous magnetic material can influence the field, as well as runout errors in the rotor shaft. These errors tend to manifest themselves as sinusoidal signal disturbances that directly track rotor speed. Disturbances tend to be at both low (one cycle per input shaft revolution) and high frequencies (integer multiples of the input shaft speed) because the tachometer is typically collocated with the torquer motor on the high side of the gear transmission. Tachometer disturbances can be described by

$$T_d = \delta K_G E_d$$

$$E_d = \sum_{n=1}^{\infty} a_n \sin(n\delta) + b_n \cos(n\delta) \tag{22}$$

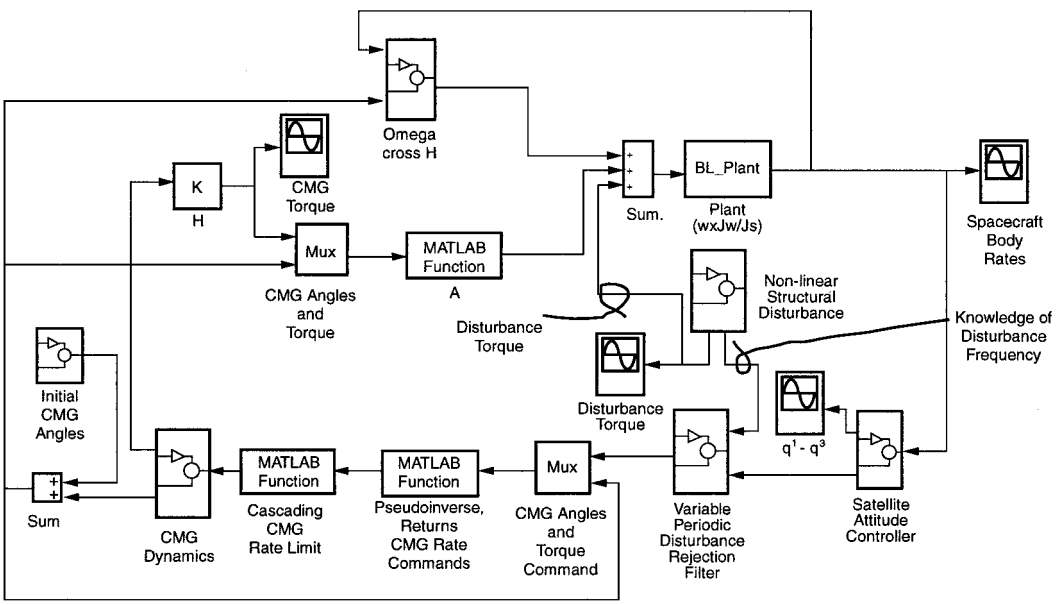

Fig. 2 Block diagram of the spacecraft model with nonlinear external disturbance.

where

T_d = disturbance torque in the gimbal axis
K_G = forward loop gain
E_d = disturbance voltage
a_n, b_n = scalar constants

There are n discrete disturbance frequencies and harmonics, where n can be large. The frequencies are phase dependent on δ, where δ is the CMG gimbal angle and the magnitude is a percentage of the CMG gimbal rate $\dot{\delta}$.

As already mentioned, the tachometer disturbance acts like sensor noise in the respect that it cannot be controlled by the feedback loop. This tends to make tachometer ripple the most predominant disturbance source in the gimbal loop.

Motor cogging occurs when the rotating motor magnets pass the stator coils, giving rise to a sinusoidal torque on the input shaft. Frequency content is dependent on the number of windings/poles in the motor, which by definition are even integers. The magnitude of the cogging torque is fixed and predominantly a function of the magnet strength. BEMF, however, is dependent on the driving current and, thereby, varies approximately as the square of the output torque. When dual-channel motors are used to phase minimize the disturbances, frequency content tends to be additive, thereby reducing the peak-to-peak disturbance, but giving rise to an additional set of harmonics at twice the fundamental. Two-phase motors driven by sinusiods tend to have very little disturbance (around 1% at the first harmonic), whereas three-phase motors driven by square waves tend to have about 16% torque ripple (peak-to-peak magnitude as a percent of the torque output of the motor). Motor commutation or switching noise can also contribute to motor torque fluctuation; however, these tend to be secondary disturbances. Motor cogging, BEMF, and commutation disturbances can be modeled similarly to the tachometer noise; however, motor cogging tends to have fixed amplitudes and are in the feedback loop where their disturbance magnitudes tend to be less than those of the tachometer.

Mechanical Errors

By nature, agile spacecraft tend to have high-platform body rates. These body rates result in a holding torque requirement on the gimbal torquer when a component of the base rate is mutually orthogonal to the spin and input axes. This holding torque is typically sufficient as to warrant a gear transmission in the gimbal torquer. The gears, although high quality, tend to have transmission errors due to multiple contributors. A partial list of error types includes: gear tooth profile, index (tooth spacing), gear tooth lead, surface finish, tooth tip relief (lack of or too much), insufficient transverse or axial contact ratio, pitchline runout, and misalignment. In addition, gear transmission errors can be generated through wear in the gears, deflections of the supporting structure, and other secondary contributions.

Transmission disturbances can be mitigated through good design and manufacturing practice; however, the effects cannot be feasibly eliminated. An interesting phenomenon of transmission error is that it tends to be worse (as a percentage of the output torque) at a lower transmitted torque.[17] The periodic component of transmission error decreases with increasing load because the hertzian contact patch increases in size, thereby increasing the effective tooth-mesh stiffness. Figure 3 shows this effect for successive tooth-mesh cycles.[18] From Fig. 3, it can be seen that, at the lower loads, the transmission error tends to be somewhat sinusoidal in nature, but then degrades toward a pseudosquare wave at higher loads. The square wave function, however, tends to be mitigated by a decrease in the disturbance amplitude with increased load (as a percentage of the transmitted torque). For practical purposes, only the disturbances at the lower loads are considered deleterious to spacecraft function and, subsequently, can reasonably be modeled as feedforward by

$$T_d = \sum_{n=1}^{\infty} a_n \sin(n\delta) \tag{23}$$

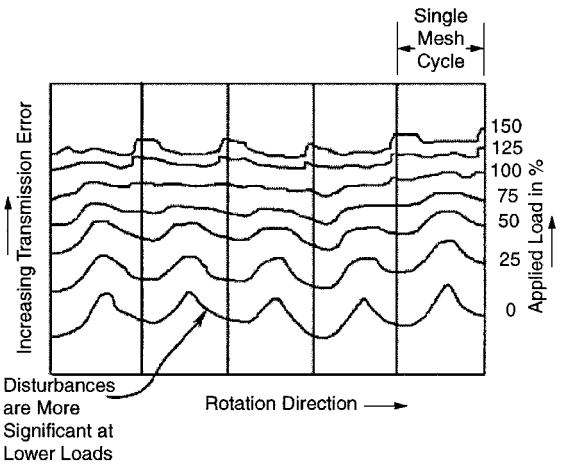

Fig. 3 Transmission error shown as displacement at tooth face for $4D_p$ spur gear mesh, 1700-lb/in. load.

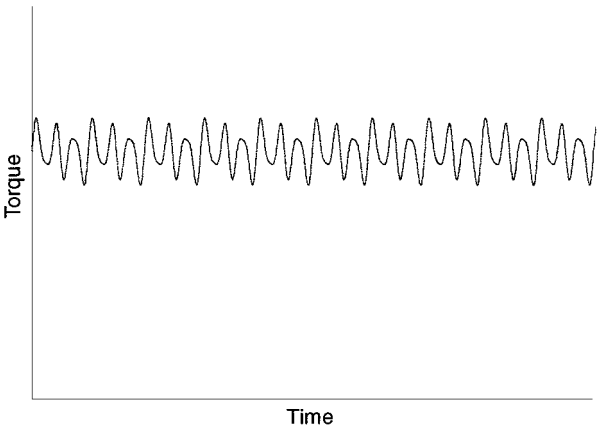

Fig. 4 Bearing torque disturbance due to race/ball imperfections.

where

T_d = disturbance torque in gimbal axis
δ = CMG gimbal angle
a_n = scalar constant at the nth gear train harmonic

Bearings in the gimbal axis can provide torque disturbances that lead to gimbal rate ripple due to variable friction and raceway/ball imperfections.[19] Raceway imperfections tend to manifest themselves as lobes at integer multiples on the inner- and outer-ball riding tracks. Because the ball speed is different from the inner and outer raceways, there are two discrete disturbances at a minimum that beat together giving rise to a lower fundamental frequency. Because the balls themselves also have nonuniform radii and can contain surface imperfections, they each tend to contribute to the disturbance at their own spin frequency, which gives rise to a fundamental (Fig. 4). Although the dc component of bearing friction is on the order of the gear disturbances, the periodic component tends to be at least an order of magnitude less. Other sources of torque fluctuation from gimbal or torquer bearings are related to the constant mixing of lubricants, typically grease. This contribution is usually at very low frequencies and magnitudes, and their disturbances can be negligible.

Both the electromechanical and mechanical CMG disturbances are dependent on the gimbal speed and angular position. For this reason, disturbances are difficult to reject using classical control techniques. The remainder of this paper, through a heuristic approach, examines the effect of sample disturbances external and internal to a point-design spacecraft. Through this approach, an improved understanding of the influence on spacecraft pointing control is achieved. It will be demonstrated that periodic disturbances of a time-variant frequency can be effectively rejected.

Accommodation of External Variable Torque

In Ref. 3, an external torque disturbance to a spacecraft was modeled as an undamped beam with a mass on its end that was retracted for the duration of 30 s. This resulted in a change in the natural frequency of the disturbance from 2 to 5 Hz. At the end of retraction, the beam was allowed to continue oscillating at 5 Hz. For that heuristic case, the disturbance was applied in only one axis. With the controller described in the "Spacecraft Attitude Control Logic" section the spacecraft attitude oscillates at the disturbance frequency with a fixed amplitude. Application of the variable periodic disturbance rejection filter (VPDRF) asymptotically drove the spacecraft rate to zero within a few seconds and tracked the disturbance for the remaining maneuver.

The VPDRF design is based on the internal model principle[20] with the capability of tracking the disturbance frequency based on knowledge of the source. In the case of the oscillating beam,[3] the disturbance source could be tracked with the rate gyros on the spacecraft, or it could be calculated with knowledge of the geometry/length of the beam. The VPDRF contains an oscillator that matches the disturbance frequency even though it constantly changes. A lightly damped zero is included to balance the system. The transfer function for this filter is given as

$$\frac{s^2 + 2\xi_i k_z f(\omega)s + [k_z f(\omega)]^2}{s^2 + 2\xi f(\omega)s + [f(\omega)]^2} \tag{24}$$

where $f(\omega)$ is a function that calculates the frequency of the periodic disturbance, k_z is a multiplier to offset the zero, and ξ and ξ_i are damping coefficients, selected as necessary to achieve the desired disturbance rejection.

To understand better the performance of this filter, two cases are explored: the effectiveness of the filter in calculating disturbance frequency in the presence of an estimation error, and the ability of the filter tracking a variable disturbance on a varied rate of change. This is accomplished by increasing the model's rate of beam retrieval (Ref. 3), and comparing the performance to the estimation error case.

The VPDRF assumes the variable periodic disturbance knowledge of the source a priori. The knowledge is used to calculate an estimation of the disturbance frequency; however, there is always some level of error associated with estimation. An error is added to the frequency estimation of the model (Ref. 3) for evaluation. In Fig. 5, the influence of 1 and 5% estimation errors on the attitude of the spacecraft are compared with zero estimation error and the baseline disturbance. It is evident from the results that, with minimal estimation error, some level of sustained periodic disturbance remains. However, when compared to the body rates under the same disturbance with no VPDRF, even 5% estimation error results in an approximate order of magnitude disturbance rejection.

Similarly, the effects of decreasing the time it takes to perform the maneuver in Ref. 3 have only a small deleterious affect on the performance. Figure 6 shows the effects of retracting the oscillating beam in 10, 5, and 2 s. When compared to the original retract time

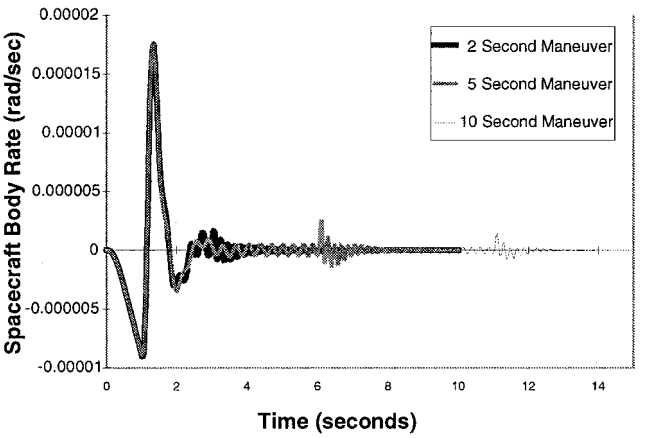

Fig. 6 Spacecraft body rate in principle axis under the influence of the disturbance of an oscillating beam being retracted in different times.

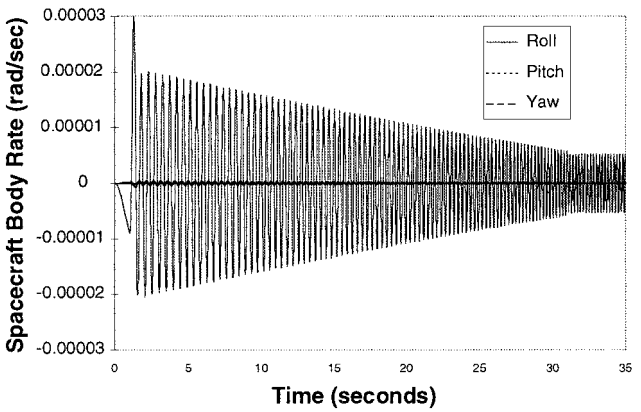

a) Under the influence of the external disturbance

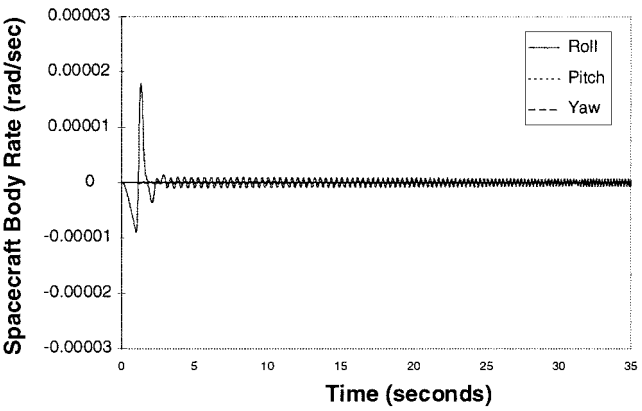

b) With VPDRF with 1% estimation error

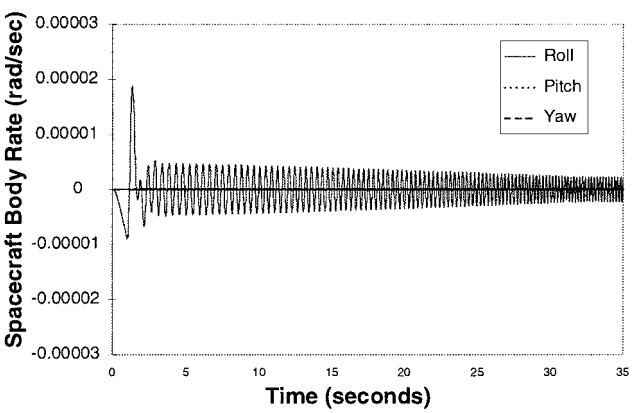

c) With 5% estimation error

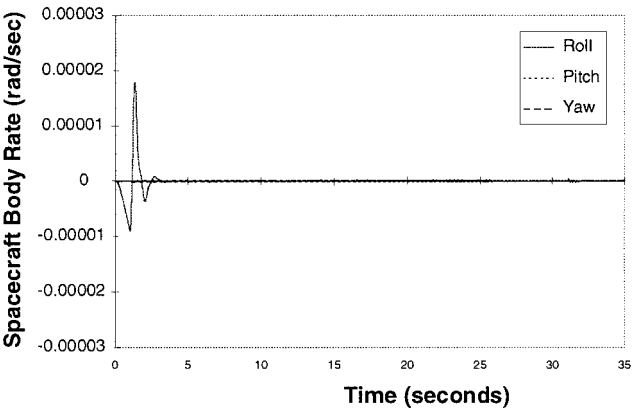

d) With no estimation error

Fig. 5 Spacecraft body rates.

(Fig. 5), it is evident that the amplitude of the sustained periodic disturbance increases only slightly with the decreased retract time.

Comparing the results of Fig. 6 to Fig. 5 gives insight into the nature of the filter. From Fig. 6, the tracking ability of the filter is influenced by the rate of change that can be expressed as being equivalent to a percent of estimation error. By examination, a rate of change in the disturbance frequency of 1.5 Hz/s is approximately equivalent to a 1% estimation error. This can be improved by increasing the bandwidth of the balancing zero in the VPDRF; however, the trade is a longer settling time.

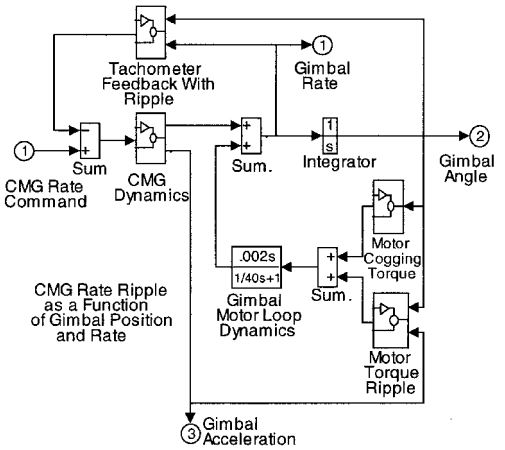

Fig. 7 Block diagram of CMG dynamics with ripple disturbance.

Accommodation of CMG Ripple Dynamics

The computer model for this investigation is similar to that used in Ref. 3 with the addition of CMG rate ripple modeled for motor and tachometer disturbances (Figs. 7–9, block diagrams). The spacecraft body rates and the CMG torque for the baseline system in the absence of disturbances (Fig. 10) given an initial quaternion displacement of $\boldsymbol{q} = (0.174, 0, 0)$ rad and a 1 deg/s spacecraft slew rate to represent a high-rate, precision-pointing maneuver. Because the system chosen has a momentum bias of $1h_0$, the gimbal angles at the end of the maneuver are different from the starting angles as a result of the system's need to preserve the bias with respect to the inertial reference. Without rate ripple disturbances in the model, the slew rates are smooth, as are the torque requirements. Note that in a zero bias system, CMG angles will remain constant during the slew. However, in the presence of a momentum bias, the CMG array maintains the bias vector throughout the maneuver, which results in changes in CMG angles. It is the errors manifested in this motion that results in rate ripple that in turn is realized as torque ripple on spacecraft.

Because torque output from the CMG array is dependent on individual momentum vector orientations, as the gimbal angles change, so do the command rates. In a CMG application, gimbal rate ripple that is realized as torque ripple is transmitted to the spacecraft as a function of the gimbal rate due to the errors described earlier. The result is a disturbance that is periodic in nature, but whose frequency

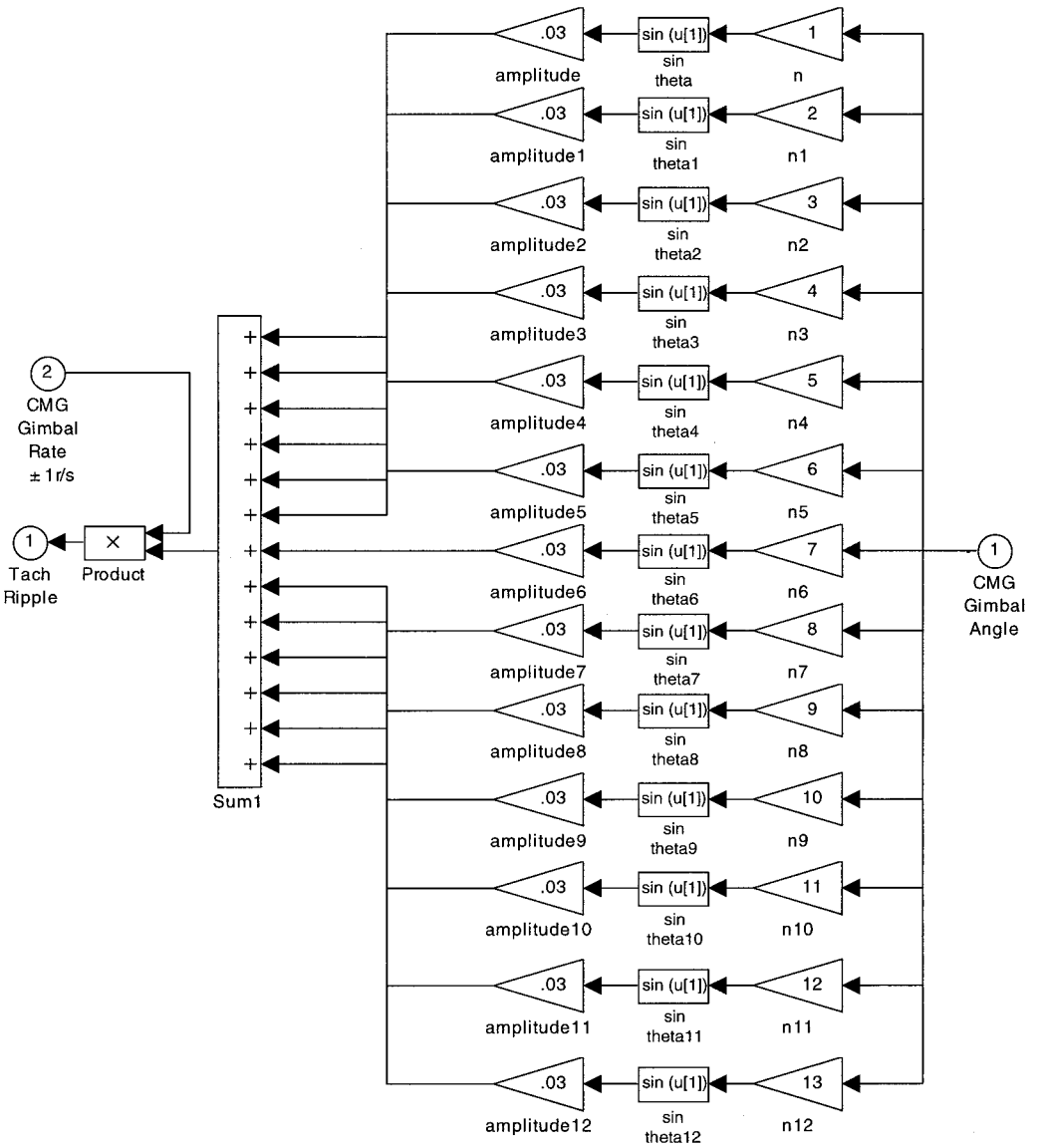

Fig. 8 Tachometer rate ripple.

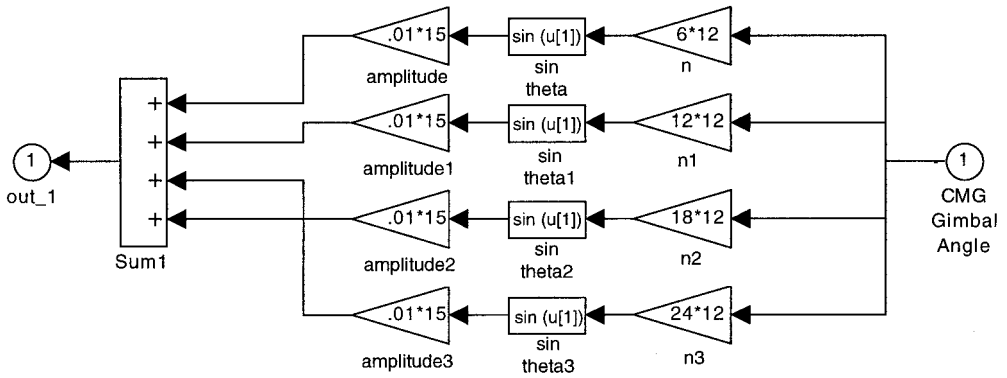

Fig. 9 Motor cogging induced-rate ripple.

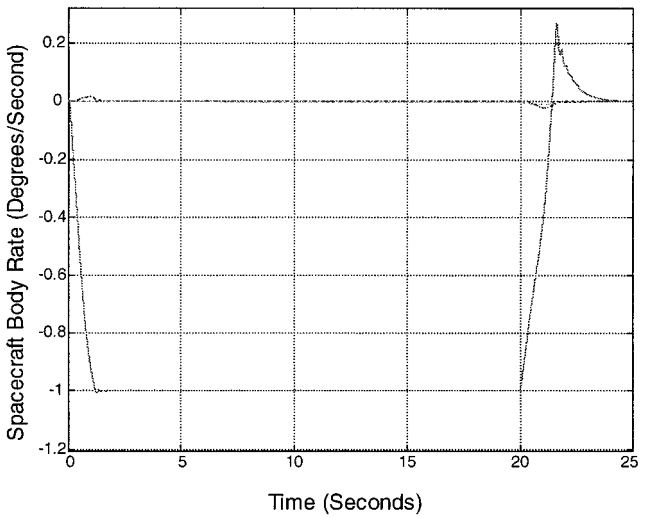

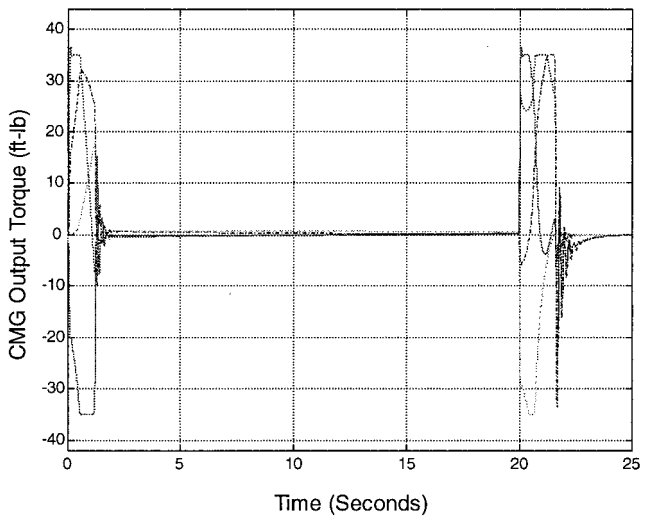

Fig. 10 Baseline slew maneuver without disturbances for q = (0.174, 0, 0).

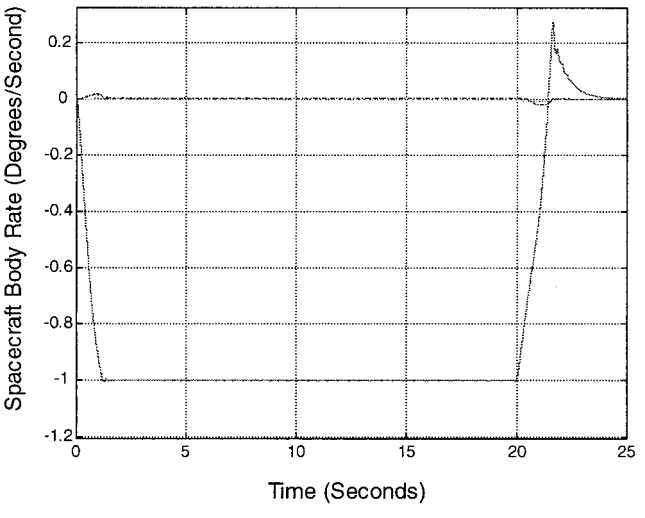

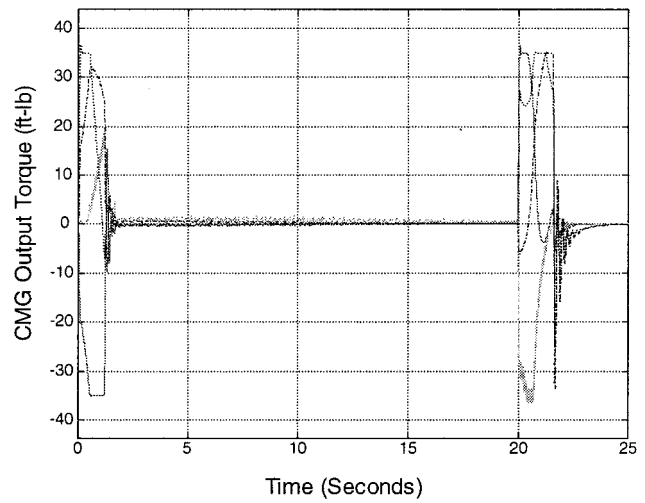

Fig. 11 Slew manuever with CMG motor disturbances for q = (0.174, 0, 0).

is constantly changing. It is during slew maneuvers when the most stable pointing requirements are typically present. Torque amplification of the ripple becomes difficult to control because the sources of the ripple (CMGs) are also the devices being used to mitigate torque disturbances.

In Ref. 3, the ripple was modeled as a feedforward effect (representative of gear noise, for example) as

$$\dot{\delta}_j \frac{\mathrm{d}}{\mathrm{d}t}[\delta_j + B_j \sin(n\delta_j)] \tag{25}$$

where

B_j = magnitude of the rate ripple at the nth harmonic
n = harmonic or multiple of the CMG rate

In that case, the ripple was effectively mitigated through the implementation of the VPDRF. However, when the ripple is modeled such that it is included in the CMG feedback loop, the problem is more pervasive in nature and much more difficult to mitigate. For the first case, the CMG disturbance was modeled as a single harmonic component of motor cogging ripple (refer to Fig. 9) that is a function

of gimbal position. The ripple is realized as a rate disturbance in the CMG forward loop, which is compounded by the feedback. The result is a disturbance that is nonlinear and does not necessarily resemble a sinusoid, but is periodic in nature. Because the ripple does not exhibit classical sinusoidal characteristics, it is more difficult for the VPDRF to reject. Figure 11 shows the highly nonlinear effect the rate ripple has on the slew maneuver. The ripple chosen here is a multiple of 720 of the gimbal angle and a magnitude of 0.5 ft · lb. This would be indicative of a gimbal motor with 720 poles. In actual practice, the poles number much less than that. However, in this heuristic case, the higher frequency affords a better visualization of the influence of CMG disturbances and demonstrates robustness with respect to the disturbance frequency rate of change.

The net impact of the CMG ripple can best be visualized by calculating the pointing error at a fixed distance. For the system described at steady state, the pointing error at an arbitrary distance of 100 miles during a portion of the slew maneuver is shown in Fig. 12.

With the addition of the variable periodic disturbance rejection filter (one for each disturbance on a CMG), the body rates are reduced, but not as well as was achieved in Ref. 3 for feedforward disturbances. The pointing error is reduced approximately an order of magnitude without exceeding the CMG output torque limit (Fig. 12). Such an improvement in motor ripple performance can allow a lower cost torque motor implementation in a CMG, i.e. utilization of a three-phase torque motor in lieu of a two-phase design.

A second case is examined for tachometer ripple. As stated earlier, tachometer ripple is analogous to sensor noise that cannot be

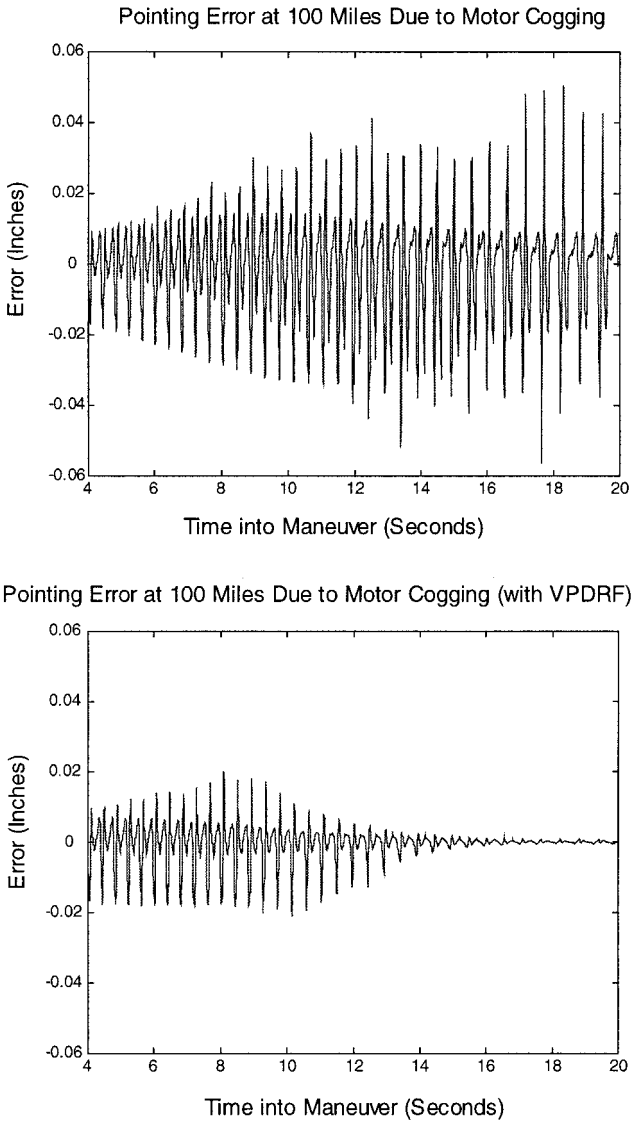

Fig. 12 Affect of VPDRF on pointing error at 100 mile.

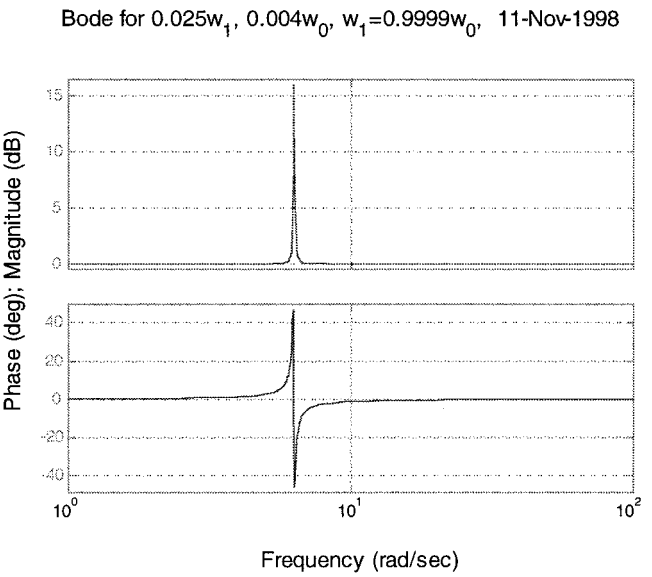

Fig. 13 Bode plot for VPDRF at an instantaneous disturbance location of 1 Hz, $k_z = 0.9999$, $\zeta_1 = 0.025$, and $\zeta_2 = 0.004$.

accommodated by the feedback loop. However, the disturbance is detected by spacecraft rate sensors, and therefore, the content is in the torque command. Implementation of the VPDRF helps mitigate the disturbance by commanding more authority to the motor at the tachometer disturbance frequency; however, the benefit is minimal because the mitigating action of the motor simply generates a higher frequency tachometer disturbance.

The influence of the VPDRF gains and bandwidth have shown that excessive gain or too wide a bandwidth is undesirable and can lead to oscillation in the absence of disturbances. Both the bandwidth and gain are most easily selected by adjusting k_z and the pole and zero damping factors. The best results for the test cases were achieved where the filter gain was between 10 and 20 and the bandwidth of the filter was less than $0.01 f(\omega)$ (Fig. 13).

Finally, note that although stability of nonlinear systems is, in the classical sense, difficult to prove directly, the filter is pointwise Lyapunov stable by design, and with proper parameter constraints, it can be shown stable over the CMG bandwidth.

Conclusions

CMG actuation of spacecraft is known to be a viable and cost effective means to control the attitude of long-life, agile spacecraft. Although previous research has addressed the implementation of CMG control laws, none of the papers on the topic specifically addressed the effects of torque ripple on the pointing performance of the spacecraft and the related control implications. In fact, the use of the CMG gives rise to time-variant (internal) torque disturbances on the host spacecraft. In the case of internal disturbances from the CMG, characterization of the rate ripple in the feedback loop was shown to be more difficult to reject than feedforward disturbances. With CMG disturbance mitigation of up to an order of magnitude demonstrated, the VPDRF has been shown to be a viable method for mitigating most internal disturbances. Consideration of this filter in the CMG control of agile spacecraft leads to the potential of reducing performance requirements of some of the CMG electromagnetic components and, thereby, the associated complexity and cost. In the case of external disturbances, the application of the VPDRF was demonstrated as extremely effective and robust. However, because most external disturbances are not time variant, this application may be moot. Stability of the filter is difficult to prove directly. However, because it can be implemented as pointwise Lyapunov stable over the CMG bandwidth, demonstration of stability can be achieved. Disturbances, linear and nonlinear, outside of the CMG control bandwidth can be effectively mitigated through structural isolation of the CMG array or spacecraft payload.

References

[1]Wie, B., and Gonzalez, M., "Control Synthesis for Flexible Space Structures Excited by Persistent Disturbances," *Journal of Guidance, Control, and Dynamics*, Vol. 15, No. 1, 1992, pp. 73–80.

[2]Wie, B., Liu, Q., and Bauer, F., Classical and Robust H_∞ Control Redesign for the Hubble Space Telescope," *Journal of Guidance, Control, and Dynamics*, Vol. 16, No. 6, 1993, pp. 1069–1077.

[3]Heiberg, C. J., Bailey, D., and Wie, B., "Precision Control Moment Gyroscope Spacecraft Control with Disturbance," Society of Photo-Optical Instrumentation Engineers, Paper 3041-93, San Diego, March 1997.

[4]Bedrossian, N. S., Paradiso, J., and Bergmann, E. V., "Steering Law Design for Redundant Single-Gimbal Control Moment Gyroscopes," *Journal of Guidance, Control, and Dynamics*, Vol. 13, No. 6, 1990, pp. 1083–1089.

[5]Vadali, S. R., Oh, H.-S., and Walker, S. R., "Preferred Gimbal Angles for Single Gimbal Control Moment Gyros," *Journal of Guidance, Control, and Dynamics*, Vol. 13, No. 6, 1990, pp. 1090–1095.

[6]Vadali, S. R., and Krishnan, S., "Suboptimal Command Generation for Control Moment Gyroscopes and Feedback Control of Spacecraft," *Journal of Guidance, Control, and Dynamics*, Vol. 18, No. 6, 1995, pp. 1350–1354.

[7]Cornick, D. E., "Singularity Avoidance Control Laws for Single Gimbal Control Moment Gyros," *Proceedings of AIAA Guidance and Control Conference*, AIAA, New York, 1979, pp. 20–33.

[8]Bedrossian, N. S., Paradiso, J. A., Bergmann, E. V., and Rowell, D., "Redundant Single Gimbal Control Moment Gyroscope Singularity Analysis," *Journal of Guidance, Control, and Dynamics*, Vol. 13, No. 6, 1990, pp. 1096–1101.

[9]Margulies, G., and Aubrun, J. N., "Geometric Theory of Single-Gimbal Control Moment Gyro Systems," *AIAA Guidance and Control Conference*, AIAA, New York, 1976, pp. 255–267.

[10]Crenshaw, J. W., "2-Speed, A Single-Gimbal Control Moment Gyro Attitude Control System," AIAA Paper 73-895, Aug. 1973.

[11]Paradiso, J. A., "Global Steering of Single Gimballed Control Moment Gyroscopes Using a Directed Search," *Journal of Guidance, Control, and Dynamics*, Vol. 15, No. 5, 1992, pp. 1236–1244.

[12]Nakamura, Y., and Hanafusa, H., "Inverse Kinematic Solutions with Singularity Robustness for Robot Manipulator Control," *Journal of Dynamic Systems, Measurement, and Control*, Vol. 108, 1986, pp. 163–171.

[13]Paradiso, J. A., "A Highly Adaptable Steering/Selection Procedure for Combined CMG/RCS Spacecraft Control," *Advances in Astronautical Sciences*, Vol. 61, Feb. 1986, pp. 263–280.

[14]Branets, V. N., Weinberg, D. M., Verestenagin, U. P., Danilov-Nirusov, N. N., Legostayev, U. P., Platonov, U. N., Semyonov, Yu. P., Semyachkin, U. S., Chertock, B. E., and Sheremetyevsky, N. N., "Development Experience of the Attitude Control System Using Single-Axis Control Moment Gyros for Long Term Orbiting Space Stations," International Astronautical Federation, Paper 87-04, Oct. 1987.

[15]Dzielski, J., Bergmann, E., Paradiso, J. A., Rowell, D., and Wormley, D., "Approach to Control Moment Gyroscope Steering Using Feedback Linearization," *Journal of Guidance, Control, and Dynamics*, Vol. 14, No. 1, 1991, pp. 96–106.

[16]Wie, B., and Lu, J., "Feedback Control Logic for Spacecraft Eigenaxis Rotations Under Slew Rate and Control Constraints," *Journal of Guidance, Control, and Dynamics*, Vol. 18, No. 6, 1995, pp. 1372–1379.

[17]Gregory, R. W., Harris, M. A., and Munro, R. G., "Dynamic Behaviour of Spur Gears," *Proceedings of the Institution of Mechanical Engineers 1963-64*, Vol. 178, Pt. 1, No. 8, pp. 207–226

[18]Townsend, D. P., *Dudley's Gear Handbook*, McGraw–Hill, New York, 1991, Chap. 14.

[19]Hightower, III, R. A., Levelle, A., and Bailey, D., "Ball Bearing Vibrations Amplitude Modeling and Test Comparisons," *Proceedings of the 4th International Rolling Element Bearing Symposium*, April 1997.

[20]Chen, C., *Linear System Theory and Design*, Holt, Rinehart and Winston, Philadelphia, 1984, p. 490.